JCTC Journal of Chemical Theory and Computation

Article

pubs.acs.org/JCTC

A Coupled Molecular Dynamics/Kinetic Monte Carlo Approach for Protonation Dynamics in Extended Systems

Gabriel Kabbe,[†] Christoph Wehmeyer,[‡] and Daniel Sebastiani*[,†]

[†]Institute of Chemistry for Physical Chemistry, Martin-Luther-University Halle-Wittenberg, von-Danckelmann-Platz 4, 06120 Halle, Germany

[‡]Institute of Mathematics, Freie Universität Berlin, Arnimallee 14, 14195 Berlin, Germany

Supporting Information

ABSTRACT: We propose a multiscale simulation scheme that combines first-principles Molecular Dynamics (MD) and kinetic Monte Carlo (kMC) simulations to describe ion transport processes. On the one hand, the molecular dynamics trajectory provides an accurate atomistic structure and its temporal evolution, and on the other hand, the Monte Carlo part models the long-time motion of the acidic protons. Our hybrid approach defines a coupling scheme between the MD and kMC simulations that allows the kMC topology to adapt continuously to the propagating atomistic microstructure of the system. On the example of a fuel cell membrane material, we validate our model by comparing its results with those of the pure MD simulation. We show that the hybrid scheme with an evolving topology results in a better description of proton diffusion than a conventional approach with a static kMC transfer rate matrix. Furthermore, we show that our approach can incorporate additional dynamical features such as the coupling of the rotation of a side group in the molecular building blocks. In the present implementation, we focus on ion conduction, but it is straightforward to generalize our approach to other transport phenomena such as electronic conduction or spin diffusion.

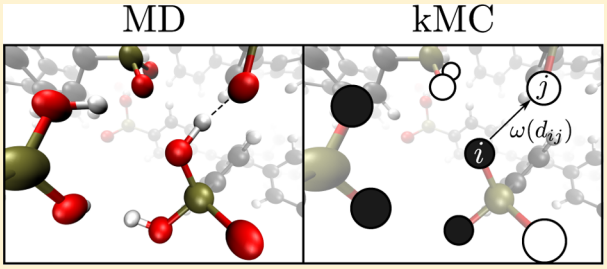

1. INTRODUCTION

Atomistic simulations of the structural parameters and the dynamical behavior of complex materials can help to gain insight into the fundamental mechanisms of many mesoscopically observable phenomena. The direct simulation of mesoscale properties, however, is often prohibitively resource-intense and can only be achieved by means of advanced simulation techniques. Here, we present a scale-bridging approach designed for the accurate description of ion transport in condensed phases; we illustrate the performance of our method on the example of proton conduction in proton exchange membrane fuel cells (PEMFC).

As the proton motion in fuel cell membranes involves the breaking of O−H bonds, methods must be applied that are able to describe chemical reactions.

While Density Functional Theory (DFT) approaches offer a good compromise between an accurate modeling of chemical bonds and universal applicability, their comparatively high computational costs typically restrict them to time scales in the picosecond range (see ref 1 for some benchmarks). Such time scales, however, are far below those required to observe the relevant processes; e.g. regarding ion conduction, only few elementary atomic hopping processes occur within a picosecond.

In order to overcome the temporal restrictions, we opted for a multiscale approach that combines a kinetic Monte Carlo scheme with DFT based MD calculations.

The combination of Monte Carlo and molecular dynamics in multiscale methods has been used before to simulate structure and dynamics in the areas of solid state physics,[2−6] polymer sciences,[7−10] or biophysics for protein folding.[11−13]

In these fields, numerous systems exhibit phenomena that are several orders of magnitude slower than the elementary atomistic processes on which they rely. To cope with such time scale-crossing questions, different types of combined MC/MD methods were developed, which can be subdivided into three classes:[14]

In *Mixed MD/MC algorithms*, some atoms are modeled by MD and the others by MC. LaBerge and Tully showed a generally applicable way to build this kind of MD/MC system.[15] Their Monte Carlo scheme uses a Metropolis algorithm[16] to model the motion of selected atoms or molecules in the whole system.

Hybrid MD/MC algorithms, on the other hand, apply a scheme that moves the atoms both deterministically and stochastically. The typical example for this type of algorithm is *Langevin Dynamics*,[17] where the equations of motion include a stochastic term.

Finally, *sequential algorithms* alternately use MD and MC steps. The MD steps model the fast processes of the system,

Received: June 4, 2014
Published: September 18, 2014

   dx.doi.org/10.1021/ct500482k | J. Chem. Theory Comput. 2014, 10, 4221−4228

whereas MC models the processes occurring on large time scales.

The examples listed so far use Monte Carlo methods similar to the Metropolis algorithm, which propose a new position in the system's configuration space per propagation step and, depending on the energy of the proposed new configuration, accept or reject it. No time information can be extracted from this kind of algorithm.

Kinetic Monte Carlo[18−20] schemes, on the other hand, are basically numerical solvers of the master equation, moving the system from one state to another according to a given transition rate. This kind of technique is used to model phenomena such as adsorption processes,[21−25] charge transport,[26] oxidation reactions[27] hydrogenation,[28] deposition processes,[29−31] crystal growth,[32−35] and diffusion processes.[36−39] In constrast to Metropolis Monte Carlo, a (real) time unit can be assigned to a number of MC steps, under the condition that the system is in a steady state.[21]

Our model can be seen as a mixture of a sequential and a mixed MD/kMC algorithm, as on the one hand, MD and kMC take turns, and on the other hand, the kMC scheme only models the dynamics of the acidic protons. The kinetic Monte Carlo scheme models the rare events, which take place on large time scales, while building its transfer rates based on the atomistic picture obtained by the MD simulation.

Our model shows good agreement with DFT calculations, and at the same time preserves time scale information within the kMC scheme. Its low computational costs allow us to extend the time scales several orders of magnitude, i.e., from picoseconds up to nano/microseconds. Its generality allows an easy transfer to other systems and phenomena.

2. METHOD

In order to reach mesoscales in a condensed phase system, we identify the parts (i.e., atomistic subsets) whose evolution takes place on a time scale not accessible for AIMD. Using a coarse-grained/simplified description by means of kMC for these slow processes allows us to significantly increase the simulation speed, while still taking into account the atomistic structure and its influence on the kMC subsystem. For an accurate description of the dynamics, we build the kMC topology from AIMD trajectories using a distance based approach.

In the following, we clarify the crucial features of our MD/kMC model. We explain the underlying Monte Carlo scheme and how to determine its rate parameters, as well as the interaction between MD and kMC model.

2.1. Kinetic Monte Carlo Scheme. *Propagation Scheme.* The kMC model used here is based on the "Asymmetric Simple Exclusion Process" (ASEP).[40] In its most basic form, the model consists of a one-dimensional lattice, whose sites can each hold one particle. At each step, a connection between two neighboring sites $(i, i + 1)$ is chosen, and if site i is occupied and site $i + 1$ is empty, the particle will hop with probability p to its right neighbor. It is straightforward to extend this model to allow jumps in both directions by adding backward connections between all node pairs. In this case, a step consists of choosing a connection (i,j), where j is either $i + 1$ or $i - 1$, and allowing a hop with probability p_{ij}. Figure 1 shows an example of a one-dimensional lattice. To establish a particle flow, either periodic boundary conditions are introduced (in Figure 1 this would mean connecting node 7 with node 1) or the system is coupled to a reservoir, which introduces particles

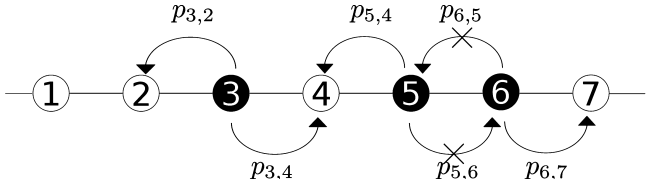

Figure 1. Illustration of a simple kMC lattice in one dimension. The particle at node 3 is allowed to jump either to the left or to the right, whereas the particles at node 5 and node 6 hinder each other's movement.

on one side with probability α and removes them from the other end with probability β.

In order to describe an actual molecular system, an ASEP model needs to be constructed, whose transfer rates and topological structure accommodate the characteristics of the considered molecule. Clearly, the neighborhood of a single node cannot be determined as trivially as in the one-dimensional example. As the linearity of the one-dimensional chain is not given anymore, every possible site pair (i,j) needs to be considered, and on the basis of the probability p_{ij} for a jump between node i and node j, it has to be decided if a jump will take place. The choice of the jump probabilities p_{ij} is crucial for the quality of our model. In section 3.2, we show a heuristic method for their determination from AIMD simulations.

Iteration Scheme and Time Step. Given the hopping rates ω_{ij} for all node pairs (i, j) of a system, with

$$\omega_{ij} = \frac{p_{ij}}{\Delta t} \tag{1}$$

a scheme must be chosen for the propagation of the particles. We use the random-sequential update,[40] which iterates over the node pairs in a random order. This means that for each propagation step a node pair (i,j) is chosen randomly, each pair having the same chance to be drawn. If N denotes the number of nodes, on average, after $N(N - 1)$ steps every node pair (i,j) was considered for a jump with probability p_{ij}. $N(N - 1)$ steps are called a sweep, and we link one sweep to the time Δt, which is determined by the hopping rates.

2.2. Coupling between Molecular Dynamics Simulation and Monte Carlo Model. The most crucial aspect of our model is the coupling between MD and the kMC algorithm, i.e. the way the kMC model obtains its topology from the MD trajectory.

For our method, a first-principles MD is performed first and then used as an input for the kMC model, which builds its rates based on the MD trajectory.

We investigated three different approaches: A Time-averaged Topology Model (TTM), which works with an averaged kMC topology, a Continuous Topology Model (CTM), which updates the kMC topology after a number of MC steps from the structure of an existing AIMD trajectory. Furthermore, we use a Shuffled Topology Model (STM), which works similarly to the CTM but draws the topologies from the trajectory in a random order.

In the following, each method will be explained in detail.

Time-Averaged Topology Model (TTM). The simplest fashion in which the MD-based structures can be incorporated within the kMC scheme is the use of an averaged topology and averaged transfer rates obtained from the MD simulation. The transfer rate matrix is given by

$$\bar{\omega}_{ij} = \langle \omega_{ij}^{k} \rangle_{k} \tag{2}$$

where ω_{ij}^{k} denotes the hopping rate between node i and node j determined from the kth frame in the MD trajectory.

The calculation of physical quantities such as the diffusion constant requires information about the spatial position of the particles. For this, an average distance matrix is determined.

$$\bar{d}_{ij} = \langle d_{ij}^{k} \rangle_{k} \tag{3}$$

where d_{ij}^{k} denotes the distance between node i and node j at the kth frame in the MD trajectory.

Continuous Topology Update Model (CTM). In an attempt to incorporate the effects of the atomic motion into our model, we deploy a scheme that updates the kMC topology regularly after a number of kMC steps.

If we denote the number of sweeps N_{MC} and the (MD) time between two subsequent topology updates T_{MD}, the loop of the CTM reads as follows:

1. Load the atomistic structure from the MD trajectory at time T
2. Determine the transfer rate matrix ω_{ij} from the new atomistic structure
3. Bridge the time ΔT_{MD} to the next update with N_{MC} sweeps of the Monte Carlo algorithm
4. $T \leftarrow T + \Delta T_{MD}$

The number of sweeps N_{MC} needed to bridge the time T_{MD} between two updates is given by

$$N_{MC} = \frac{\Delta T_{MD}}{\Delta t} \tag{4}$$

where Δt is the temporal unit obtained from the jump rates.

Only the transfer rates are updated when a new atomistic structure is loaded from the MD trajectory. This means that the current proton occupation state in the kMC model is not affected by this change in topology. When the end of the MD trajectory is reached, the CTM will continue by loading further atomistic structures from the beginning of the trajectory again.

Shuffled Topology Update Model (STM). In a different approach, the temporal order of the MD trajectory is abandoned, and the configurations are extracted in a random fashion. The loop of the STM consists of the following steps:

1. Draw a random integer $r \in (1, N_{traj})$.
2. Load the atomistic structure from frame r in the trajectory.
3. Determine the transfer rate matrix ω_{ij} from frame r.
4. Let the kMC algorithm run for N_{MC} sweeps.

where N_{traj} is the number of frames in the trajectory.

In this approach, N_{MC} cannot be determined as straightforwardly as in the CTM because of the loss of temporal coherence between successively drawn topologies. We chose to use 75 sweeps after each topology update.

3. RESULTS

3.1. AIMD Trajectories. We apply our MD/kMC model to a columnar supramolecular assembly consisting of eight 6(*p*-phosphonatophenyl)benzene (*p*-6 PA-HPB) molecules. These molecules have a disk-like shape and exhibit phosphonic groups at their edges. Because of their shape they arrange in hexagonal stacks, forming channels that promote proton diffusion. This makes them well suited for use as PEM fuel cell membranes.

The trajectories of *p*-6 PA-HPB were run over a time scale of 30 ps at 400, 500, and 600 K.[41] We use these three trajectories to build a heuristic model of our jump rates (see section 3.2) and use the temporal change of the molecular topologies to build a time-dependent transfer rate matrix for our kinetic Monte Carlo model.

3.2. Determination of a Jump Rate from AIMD. We want to transfer the dynamic behavior of the protons in the MD simulation onto our Monte Carlo model. Assuming a dependence of the transfer rate solely on the donor−acceptor distance, i.e.

$$\omega_{ij} = \omega(d_{ij}) \tag{5}$$

we evaluate the proton transfer rate between oxygen pairs at different distances:

1. At time t, count the number of oxygen pairs $N_{ox}(d,t)$ at a distance d (or more precisely within an interval $[d - \Delta d/2, d + \Delta d/2]$) that may be possible candidates (i.e. all donoracceptor pairs).
2. At time $t + \Delta t$, determine the number of jumps $N_{jump}(d, t + \Delta t)$ that occurred between them.

The quotient $N_{jump}(d, t + \Delta t)/N_{ox}(d,t)$ will then give the probability for a jump if two oxygens are a distance d apart. We chose a binwidth $\Delta d = 0.01$ Å for the resulting histogram. By averaging this ratio over the whole trajectory, a distribution (see Figure 2. Thus, we fit it accordingly via

$$\omega(d) = \frac{a}{1 + \exp\left(\frac{d-b}{c}\right)} \tag{6}$$

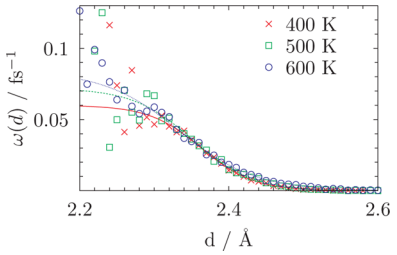

Figure 2. Fit of the jump rates at 400, 500, and 600 K using a step function.

The resulting fit parameters can be found in Table 1. As the transfer rate describes the probability of a proton jump between two successive frames, its temporal unit is determined by the time step of the trajectory.

Table 1. Parameters of the Fermi Fit for the 30 ps Trajectories

T/K	a/fs^{-1}	b/Å	c/Å^{-1}
400	0.060(3)	2.363(5)	0.035(2)
500	0.072(5)	2.351(7)	0.040(3)
600	0.084(5)	2.334(6)	0.051(2)

In Figure 2, the resulting transfer rates are plotted (including the curves of the Fermi fit as straight lines). A similar behavior for all three temperatures can be seen. At larger distances, the Fermi curve's tail increases with temperature and therefore promotes long-range proton transfer.

Figure 2 shows strong fluctuations of the transfer rate at oxygen distances smaller than 2.3 Å. The reason for this is that both the number of proton jumps and the number of oxygen pairs at this distance is very small. Therefore, only a few hopping events can be sampled there.

Symmetry of the Transfer Rate Matrix. The ASEP method mentioned before allows connections between two nodes i and j such that the probability for a jump from i to j, p_{ij}, and the probability for a jump back, p_{ji}, are different. In other words, it is possible to construct an asymmetric transfer rate matrix.

Our choice to determine the transfer rate by a distance dependent function ensures a symmetric transfer rate function, though. This is due to the fact that the distance matrix d_{ij} is symmetric, and therefore $\omega_{ij} = \omega(d_{ij})$ must be symmetric as well.

3.3. Activation Energy of a Proton Jump. While the jump rates obtained in section 3.2 show a similar behavior from 400 to 600 K, a more thorough examination reveals a slight increase of the jump rate with temperature. This temperature dependence is reflected by the Arrhenius equation

$$\omega = A \exp\left(-\frac{E_a}{RT}\right) \tag{7}$$

which allows us to determine the activation energy from ω via

$$E_a(d) = -R\frac{\partial(\ln(\omega(d)))}{\partial\left(\frac{1}{T}\right)} \tag{8}$$

The result in Figure 3 shows that the activation energy stays low at oxygen distances below 2.4 Å but rises quickly afterward.

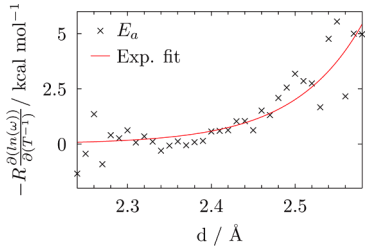

Figure 3. Exponential fit of the activation energy as a function of the O−O distance.

We fitted the data in the range from 2.24 to 2.58 Å with an exponential function

$$E_a(d) = \exp(ad + b) \tag{9}$$

with a = 12.4 Å^{-1} and b = −30.3.

For a typical O−O distance in a hydrogen bond between 2.5 and 2.6 Å, the resulting activation energy is then between about 2 and 7 kcal/mol. This is on the same order of magnitude as the energy barrier of proton transfer in liquid water.[42]

3.4. Topological Adjustments. In order to describe the proton transport in *p*-6 PA-HPB well, the purely distance-based approach needed to be modified slightly. This is due to the fact that no proton jumps are observed between oxygens within the same phosphonic group, although the distance-based criterion would allow them. Therefore, all edges between such oxygens were manually set to zero. Especially in anisotropic systems, care must be taken not to allow proton transfer between oxygens that do not show proton transfer in the DFT trajectory.

3.5. Proton Dynamics in a Nondriven Setting. We compared our MD/kMC model with original DFT trajectories (see section 3.1), which consisted of a fully periodic system of eight *p*-6 PA-HPB disks arranged in two layers. Both AIMD and kMC model hold a total number of 96 protons.

In order to verify that the MD/kMC model's dynamic behavior shows a reasonable agreement with the original AIMD results, we compare the evolution of the covalent bond autocorrelation function and the mean square displacement (MSD) for the different models.

Both for the autocorrelation function of the covalent bonds and the MSD, the MD/kMC hybrid results were averaged over 100 disjunct intervals, whereas the MD trajectory was averaged over 20 overlapping intervals.

Evolution of Covalent Bonds. In order to quantify the proton dynamics within the molecular system, we observe the change of covalent bonds between oxygens and protons over time. For this, we define a vector $\mathbf{H}(t)$, which, for each acidic proton in the system at time t, holds the index of its covalent bonding partner. In the case of the AIMD trajectories, we store the indices of each proton's nearest oxygen neighbor, whereas for the MD/kMC model, the indices of the oxygen sites at which the protons are residing, are saved.

The quantity

$$\eta_{cov}(t) = \left\langle \sum_i \delta_{H_i^{cov}(t_0), H_i^{cov}(t+t_0)} \right\rangle_{t_0} \tag{10}$$

reduces the multidimensional vector $\mathbf{H}(t)$ to a scalar value by counting the covalent bondings that have not changed since time t_0.

The progress of $\eta_{cov}(t)$ is shown in Figure 4a−c. While the kinetic Monte Carlo models show qualitatively a similar development of $\eta_{cov}(t)$ to the AIMD, the kMC models decay faster than the AIMD simulation. But we can also observe that the CTM stays closest to the AIMD, whereas TTM and STM show a very similar decay whose difference to the AIMD clearly grows with increasing temperature.

In order to explain the different dynamic behavior of the MD/kMC models, one has to keep in mind how each model's topology changes over time and how this affects the proton paths. Whenever two oxygen atoms are closer than around 2.4 Å, the fitted step function (see Figure 2) shows a relevant hopping probability. Jumps to more distant oxygen atoms on the other hand are very unlikely. Because of the smoothly changing topology of the CTM, new proton paths will only appear after some time. The TTM on the other hand, provides many possible proton paths for each oxygen at every time step because of its time averaged connectivity matrix. This increases the mobility of each proton and leads to a stronger decline of $\eta_{cov}(t)$.

In the case of the STM, the observed behavior depends on the number of sweeps used between two topology updates. While we used a number of 75 sweeps for the results presented here, we could observe that a variation of the number of sweeps results in either a behavior similar to the TTM (if a small sweep number is used) or one similar to the CTM for large sweep numbers. This behavior is reasonable, as a small topology update interval results in quickly changing proton paths, which promotes a fast change of the covalent bondings. Large update intervals, in contrast, keep one topology fixed for a longer time, which results in a behavior similar to the CTM.

Mean Square Displacement. We compare the dynamics of the AIMD trajectories and our MD/kMC model on the basis of

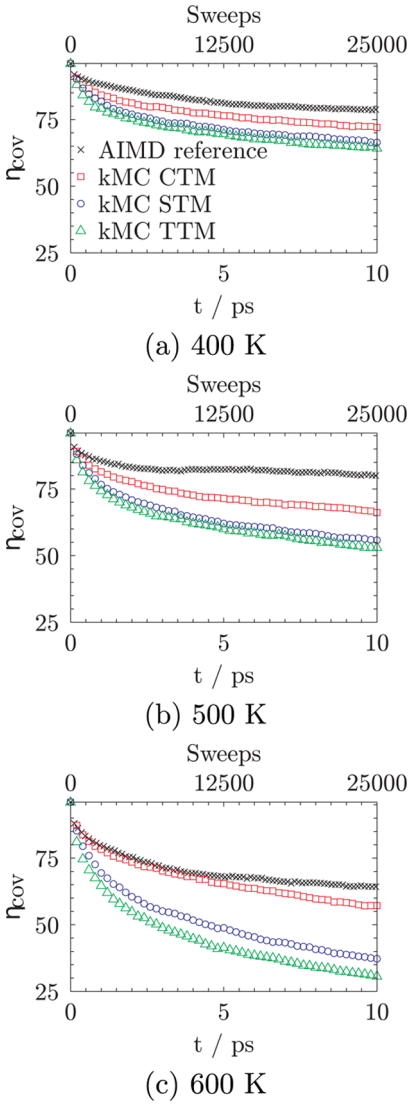

Figure 4. Autocorrelation of the covalent O−H bonds based on DFT trajectory (×), dynamic MD/kMC model (□), dynamic MD/kMC model using a shuffled topology update (○), and MD/kMC model with averaged transition rates (△).

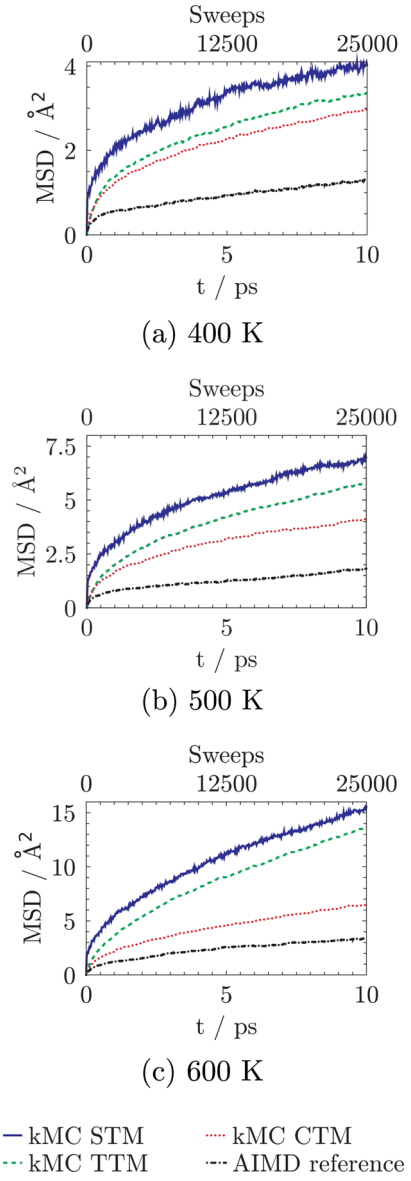

Figure 5. Mean squared displacement of the acidic protons based on DFT trajectory (black), continuous topology model (red), shuffled topology model (blue), and time-averaged topology model (green).

the MSD. Although the MD/kMC model allows us to sample the MSD over larger intervals than for the AIMD simulations, we restrict them to 10 ps at first, for a direct comparison.

In Figure 5a−c, the MSD is shown for the three Monte Carlo models and the AIMD simulation. At all three temperatures, the Monte Carlo models show a higher MSD than the AIMD, with the STM having the largest MSD, followed by the TTM and the CTM. The overestimation of the Monte Carlo models is due to the fact that the minimal distance a kMC proton can travel is the distance between two neighboring oxygens. This increases the distance of a proton jump by about 2 Å (if we assume that a hopping proton in the AIMD keeps a distance of 1 Å to its covalent bonding partners). Consequently, the MSD is overestimated at short time scales but levels in the long run.

In the next step, we take the conductivity obtained from the AIMD as a reference and compare the conductivities of the kMC models, sampled over an interval of 150 ps, with it. We determine the diffusion constant D via

$$\langle(\mathbf{r}(t + t_0) - \mathbf{r}(t_0))^2\rangle_{t_0} = 6Dt \tag{11}$$

by fitting the slope of the MSD from 20 to 150 ps. The conductivity is determined from the diffusion constant via

$$\sigma = \frac{De^2n}{k_BT} \tag{12}$$

A look at the MSD of the kMC models shows that the slope of the MSD has not leveled yet; i.e., if we were to determine the diffusion constants from a 10 ps interval, the resulting values would be clearly larger than the ones obtained from a 150 ps interval. We expect the same behavior for the AIMD. Therefore, the following comparison should only be considered as a trend of the kMC models with respect to the AIMD.

The diffusion constants of the kMC models show a smaller conductivity for 400 and 500 K than the AIMD. At 400 K, the conductivities of all three models are about 30% of the AIMD's conductivity. At 500 K, the conductivity of the CTM shows the lowest value (about 60%), followed by the STM (about 75%). The conductivity of the TTM shows the best agreement with

dx.doi.org/10.1021/ct500482k | J. Chem. Theory Comput. 2014, 10, 4221−4228

the AIMD result (about 85%). At 600 K, both TTM and STM show a conductivity about 2 times as high as that of the AIMD (TTM, 225%; STM, 170%). The conductivity of the CTM, in contrast, stays below the AIMD's conductivity (75%).

We see that the difference between the kMC models strongly varies with temperature. While at low temperatures, all three models behave very similarly, their behavior diverges with increasing temperature. Only the CTM stays close to the AIMD, whereas TTM and STM strongly overestimate the MSD.

Jump Rates. We compare the dynamics of the original DFT simulation and our MD/kMC model by counting the jumps of the 96 protons occurring in the MD/kMC model and in the MD trajectory and dividing them by the time each system was measured. The comparison shows that the total number of jumps observed within 1 ps in the MD/kMC models is about a quarter of that of the MD trajectory. This ratio stays almost constant with varying temperature.

As Table 2 shows, the numbers of proton jumps that can be observed in the MD/kMC models do not match those of the AIMD exactly. But this is not surprising, as our fit function used for the determination of the jump rates (Figure 2) is only a heuristic approximation, which, especially for small oxygen distances, lacks accuracy, which is caused by the small sampling. Furthermore, a model error is introduced by describing the proton dynamics solely through the ASEP model (section 2.1). Thus, we think that the results are still in good agreement with the original AIMD outcome.

Table 2. Jump Rates of MD/kMC Models and MD (in ps^{-1})

model	400 K	500 K	600 K
MD	212(3)	280(3)	417(4)
TTM	58.2(2)	78.8(3)	115.4(3)
CTM	53.7(2)	77.8(3)	113.8(3)
STM	56.3(2)	75.7(3)	115.2(3)

3.6. MD/kMC in a Driven Setting. We examine the proton conduction behavior of *p*-6 PA-HPB in a driven setting. For this, we set up our system such that four stacks, each with 10 molecules, form proton channels along the z axis. The system is periodic in x and y directions, and a proton flux along the z axis is triggered by a reservoir, which couples to the molecular system through two sinusoidal functions $\alpha(z)$ and $\beta(z)$.

$$\alpha(z) = \frac{1}{2}\left[1 + \cos\left(\frac{z - z_{\min}}{\lambda}\pi\right)\right] \tag{13}$$

with $z_{\min} \le z \le z_{\min} + \lambda$ and

$$\beta(z) = \frac{1}{2}\left[1 + \cos\left(\frac{z_{\max} - z}{\lambda}\pi\right)\right] \tag{14}$$

with $z_{\max} - \lambda \le z \le z_{\max}$.

While on one side protons are added with the probability $\alpha(z)$ per time step (see Figure 6, bottom picture on the left), they are withdrawn on the other side with the probability $\beta(z)$. We set the parameter λ, which defines the depth of proton insertion and proton withdrawal to 6 Å.

In order to describe the proton flux in the case of a coupled reservoir, we use a collective coordinate $R_z(t)$ that sums up the vectorial distances the protons in the system cover over time.

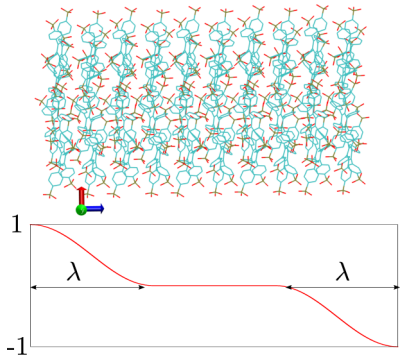

Figure 6. Upper picture: Supramolecular structure of the proton conducting material *p*-6 PA-HPB. Here, protons are added on the left side and withdrawn on the right side. Lower picture: Probability for proton insertion (left side) and proton withdrawal (right side), respectively. λ denotes the range in which protons can be added or taken from the lattice. We set it to 6 Å.

$$R_z(t) = \int_0^t \mathrm{d}t' \sum_{p \in S_t'} \Delta r_{z,p}(t') \tag{15}$$

S_t denotes the set of protons that are found in the system at time t, and $\Delta r_{z,p(t)}$ is the distance proton p moves at time t along the z axis.

This quantity can be used to quantify the overall proton movement through the system.

With the setting described above, we investigate the proton conduction along the columnar direction of our system.

Influence of the PO(OH)$_2$ Rotations. We want to determine which influence an increase of the rotation rates of the phosphonic groups of our test system has on the proton conductivity. For this, we define a rotation event in the Monte Carlo model, which swaps protons residing in one phosphonic group cyclically with a rate ω_{rot}.

Figure 7 shows the resulting variations in proton flux when the probability for a phosphonic group's rotation is increased. The kMC model used here is the CTM.

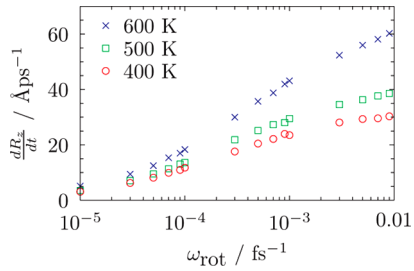

Figure 7. Response of the proton flux to variation of the rotation rates. For each rotation rate, 10 runs were averaged.

When plotting the slope of R_z over ω_{rot} (Figure 7), it can be observed that for all three temperatures the proton motion in the z direction increases upon increasing rotation frequencies. At 600 K, higher rotation rates show a greater influence on the proton flux, whereas both the 400 K and the 500 K curves get close to a plateau near $\omega_{\mathrm{rot}} = 0.01$ fs^{-1}. The plateau is reached when ω_{rot} exceeds the proton jump rate, which then becomes the rate-determining step.

This setup shows the importance of the phosphonic rotations for the proton conduction in our test system *p*-6 PA-HPB. It also illustrates how the kMC model is able to predict trends of

dx.doi.org/10.1021/ct500482k | J. Chem. Theory Comput. 2014, 10, 4221−4228

the proton conduction if the underlying structure of a molecular system changes.

Average Density. In order to gain insight into the spatial proton distribution as a result of the connected proton reservoir, the average occupation density of the oxygen sites was plotted in Figure 8a–c, i.e. the ratio of protons found and

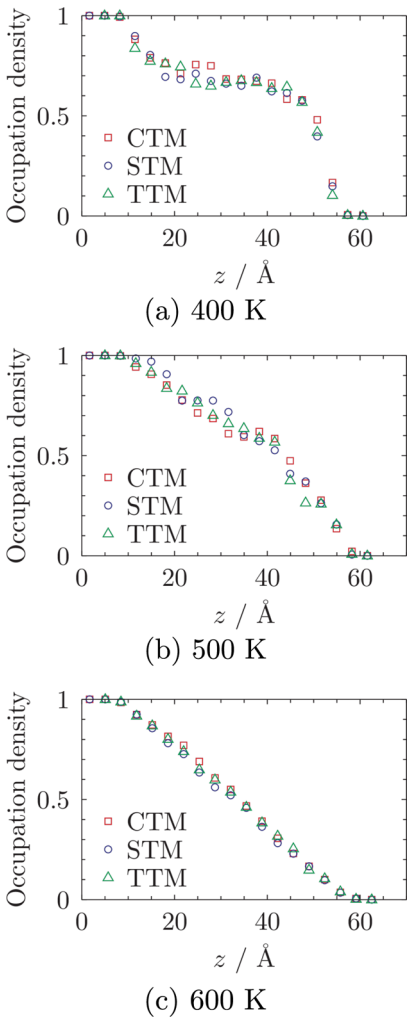

Figure 8. Relative excess proton density profile along the z axis (i.e., along the columnar stacks) at different temperatures. The proton insertion/deletion regions extend λ = 6 Å into the stack.

available oxygen sites in an interval along the z axis. We averaged the density distribution over an interval of 5×10^6 sweeps after an equilibration time of 5×10^6 sweeps.

All three models exhibit basically the same density profile. At 400 K, the density flattens in the middle region. This is in agreement with the low diffusion we could observe in the nondriven setting in section 3.5. At 500 K, the plateau has almost completely vanished, and at 600 K the densities of all three models diminish linearly from source to drain.

4. CONCLUSION

We developed a hybrid MD/kMC approach using a kinetic Monte Carlo scheme whose topology dynamically adapts to the atomistic structure of an MD trajectory. The hybrid scheme is capable of taking the atomistic structure into account while still allowing to extend the time scales by several orders of magnitude.

A heuristically determined hopping rate function allows us to build kMC topologies based on the molecular structure of complex underlying systems.

We tested different approaches to link the Monte Carlo method with the AIMD, using a model with a fixed topology and fixed transfer rates, a dynamic model that updates its underlying oxygen topology after fixed kMC steps with randomly drawn states from the AIMD trajectory and a dynamic model that updates the oxygen topologies sequentially from the AIMD trajectory. While all three models show qualitatively similar results, the CTM showed the best agreement with the AIMD results, whereas both TTM and STM overestimate the decay of covalent bondings and the MSD in a direct comparison. However, fine-tuning of the kMC time of the STM can yield results similar to the CTM.

A particularly noteworthy aspect of our method is that the proton dynamics can be well described by a function of the distance that depends only on three parameters. Compared to other scale-briding methods, the ease of use is a big advantage and makes our method ideal for a first estimation of the proton conduction properties in molecular systems. Furthermore, the ease of manipulating the underlying structure allows one to fathom how changes in the network of proton paths will alter the overall behavior of the conductivity. As an example, we showed how the rotational coupling of the side groups influences the overall proton conductivity.

Nevertheless, there are still shortcomings that need to be addressed in the future. The extraction of $\omega(d)$ from an MD trajectory is nontrivial due to the difficulty of determining the exact cause of a proton jump. For a more exact hopping rate, further parameters, such as the angle between the functional groups should be taken into account. Furthermore, our model neglects long-range correlations between the excess protons. In particular, the hopping rate of a proton should be influenced by the occupation numbers of the nearby oxygens. At the moment, only the exclusion principle of the ASEP is applied. Finally, our model lacks feedback from the kMC algorithm to the MD so far. Therefore, the MD structure will not adapt to the current proton occupation in the kMC model.

■ ASSOCIATED CONTENT

Supporting Information

Jump rates in the AIMD trajectory, fit parameters of the covalent bond autocorrelation, diffusion constants of the nondriven setting. This material is available free of charge via the Internet at http://pubs.acs.org.

■ AUTHOR INFORMATION

Corresponding Author

*E-mail: daniel.sebastiani@chemie.uni-halle.de.

Notes

The authors declare no competing financial interest.

■ ACKNOWLEDGMENTS

This work has been supported by the German Research Foundation (DFG) under Grant Se1008/6-2.

■ REFERENCES

(1) VandeVondele, J.; Krack, M.; Mohamed, F.; Parrinello, M.; Chassaing, T.; Hutter, J. *Comput. Phys. Commun.* **2005**, *167*, 103–128.
(2) Hiwatari, Y.; Kaneko, Y.; Mikami, T.; Ohara, K.; Asa, F. *Mol. Simul* **2007**, *33*, 133–138.

(3) Betz, G.; Husinsky, W. *Nucl. Instrum. Methods Phys. Res., Sect. B* **2002**, *193*, 352−358.
(4) Knizhnik, A.; Bagaturyants, A.; Belov, I.; Potapkin, B.; Korkin, A. *Comput. Mater. Sci.* **2002**, *24*, 128−132.
(5) Kaneko, Y.; Mikami, T.; Hiwatari, Y.; Ohara, K. *Mol. Simul.* **2005**, *31*, 429−433.
(6) Ghoufi, A.; Maurin, G. *J. Phys. Chem. C* **2010**, *114*, 6496−6502.
(7) Forrest, B. M.; Suter, U. W. *J. Chem. Phys.* **1994**, *101*, 2616−2629.
(8) Gromov, D. G.; de Pablo, J. J. *J. Chem. Phys.* **1995**, *103*, 8247−8256.
(9) Irbäck, A. *J. Chem. Phys.* **1994**, *101*, 1661−1667.
(10) Heermann, D. W.; Yixue, L. *Macromol. Theory Simul.* **1993**, *2*, 299−308.
(11) Hansmann, U. H.; Okamoto, Y. *Curr. Opin. Struct. Biol.* **1999**, *9*, 177−183.
(12) Zhang, H. *Proteins: Struct., Funct., Bioinf.* **1999**, *34*, 464−471.
(13) Peter, E. K.; Shea, J.-E. *Phys. Chem. Chem. Phys.* **2014**, *16*, 6430−6440.
(14) Neyts, E.; Bogaerts, A. *Theor. Chem. Acc.* **2012**, *132*, 1−12.
(15) LaBerge, L. J.; Tully, J. C. *Chem. Phys.* **2000**, *260*, 183−191.
(16) Chib, S.; Greenberg, E. *Am. Stat.* **1995**, *49*, 327−335.
(17) Lemons, D. S.; Gythiel, A. *Am. J. Phys.* **1997**, *65*, 1079−1081.
(18) Young, W. M.; Elcock, E. W. *Proc. Phys. Soc.* **1966**, *89*, 735.
(19) Bortz, A.; Kalos, M.; Lebowitz, J. *J. Phys. Chem.* **1975**, *17*, 10−18.
(20) Gillespie, D. T. *J. Phys. Chem.* **1976**, *22*, 403−434.
(21) Chatterjee, A.; Vlachos, D. *J. Comput. Aided Mater. Des.* **2007**, *14*, 253−308.
(22) Henkelman, G.; Jónsson, H. *J. Chem. Phys.* **2001**, *115*, 9657−9666.
(23) Claassens, C. H.; Terblans, J. J.; Hoffman, M. J. H.; Swart, H. C. *Surf. Interface Anal.* **2005**, *37*, 1021−1026.
(24) Nath, P.; Ranganathan, M. *Surf. Sci.* **2012**, *606*, 1450−1457.
(25) Antoshchenkova, E.; Hayoun, M.; Finocchi, F.; Geneste, G. *Surf. Sci.* **2012**, *606*, 605−614.
(26) Kim, K. S.; Hwang, Y. W.; Lee, H. G.; Won, T. Y. *J. Nanosci. Nanotechnol.* **2014**, *14*, 5839−5843.
(27) Noussiou, V.; Provata, A. *Surf. Sci.* **2007**, *601*, 2941−2951.
(28) Mei, D.; Sheth, P. A.; Neurock, M.; Smith, C. M. *J. Catal.* **2006**, *242*, 1−15.
(29) Treeratanaphitak, T.; Pritzker, M. D.; Abukhdeir, N. M. *Electrochim. Acta* **2014**, *121*, 407−414.
(30) Zheng, X.-J.; Yang, B.; Zhu, Z.; Wu, B.; Mao, Y.-L. *Trans. Nonferrous Met. Soc. China* **2007**, *17*, 1441−1446.
(31) Liu, J.; Liu, C.; Conway, P. P. *Electrochim. Acta* **2013**, *97*, 132−142.
(32) High-Performance Computing in Science: Kotrla, M. *Comput. Phys. Commun.* **1996**, *97*, 82−100.
(33) Rak, M.; Izdebski, M.; Brozi, A. *Comput. Phys. Commun.* **2001**, *138*, 250−263.
(34) Dai, J.; Seider, W. D.; Sinno, T. *Mol. Simul* **2007**, *33*, 733−745.
(35) Zhu, P.; Smith, R. *Acta Mater.* **1992**, *40*, 683−692.
(36) SSPC-16 Conference Proceedings {SSI} Special Issue: Hermet, J.; Bottin, F.; Dezanneau, G.; Geneste, G. *Solid State Ionics* **2013**, *252*, 48−55.
(37) Dholabhai, P. P.; Anwar, S.; Adams, J. B.; Crozier, P.; Sharma, R. *J. Solid State Chem.* **2011**, *184*, 811−817.
(38) Kang, J.-W.; Kwon, O. K.; Lee, S.; Lee, S. H.; Kim, D. H.; Hwang, H.-J. *J. Comput. Theor. Nanosci.* **2010**, *7*, 604−611.
(39) Lee, E.; Prinz, F. B.; Cai, W. *Electrochem. Commun.* **2010**, *12*, 223−226.
(40) Rajewsky, N.; Santen, L.; Schadschneider, A.; Schreckenberg, M. *J. Stat. Phys.* **1998**, *92*, 151−194.
(41) Wehmeyer, C.; Schrader, M.; Andrienko, D.; Sebastiani, D. *J. Phys. Chem. C* **2013**, *117*, 12366−12372.
(42) Komatsuzaki, T.; Ohmine, I. *Chem. Phys.* **1994**, *180*, 239−269.